JOURNAL OF SYNCHROTRON RADIATION
ISSN 1600-5775

A simple optical system delivering a tunable micrometer pink beam that can compensate for heat-induced deformations

Ruben Reininger,* Zunping Liu, Gilles Doumy and Linda Young

Advanced Photon Source, Argonne National Laboratory, Argonne, IL 60439, USA.
*Correspondence e-mail: rreininger@anl.gov

Received 9 January 2015
Accepted 31 March 2015

Edited by P. A. Pianetta, SLAC National Accelerator Laboratory, USA

Keywords: ray tracings; pink beam; undulator radiation; microfocusing; heat load.

The radiation from an undulator reflected from one or more optical elements (usually termed 'pink-beam') is used in photon-hungry experiments. The optical elements serve as a high-energy cutoff and for focusing purposes. One of the issues with this configuration is maintaining the focal spot dimension as the energy of the undulator is varied, since this changes the heat load absorbed by the first optical element. Finite-element analyses of the power absorbed by a side water-cooled mirror exposed to the radiation emitted by an undulator at the Advanced Photon Source (APS) and at the APS after the proposed upgrade (APSU) reveals that the mirror deformation is very close to a convex cylinder creating a virtual source closer to the mirror than the undulator source. Here a simple optical system is described based on a Kirkpatrick–Baez pair which keeps the focus size to less than 2 μm (in the APSU case) with a working distance of 350 mm despite the heat-load-induced change in source distance. Detailed ray tracings at several photon energies for both the APS and APSU show that slightly decreasing the angle of incidence on the mirrors corrects the change in the 'virtual' position of the source. The system delivers more than 70% of the first undulator harmonic with very low higher-orders contamination for energies between 5 and 10 keV.

1. Introduction

Photon-hungry experiments which do not require high-energy-resolution X-rays, *e.g.* time-resolved (Eybert *et al.*, 2002; Coppens *et al.*, 2010; Graber *et al.*, 2011; March *et al.*, 2015), imaging and tomography (Bohic *et al.*, 2001; Rau *et al.*, 2007; Kosior *et al.*, 2012; Kohn *et al.*, 2013), high-pressure emission spectroscopy (Shen *et al.*, 2008), use a 'pink-beam', the radiation from an undulator filtered by the reflection from a grazing-incidence mirror coated with the appropriate reflecting material. As is well known, the power emitted by an undulator varies significantly as the resonant photon energy is tuned by changing the k value of the insertion device (Elleaume, 1992). This in turn means that the power absorbed by the optics changes and, consequently, the optics shape. Therefore, changing the energy emitted by the undulator will have an effect on the spot size at the experiment.

An additional optical element, *e.g.* a bendable mirror (Susini *et al.*, 1992; Sutter *et al.*, 2012; Idir *et al.*, 2010; Cocco *et al.*, 2010) downstream of the deformed optic, can be used to compensate for the defocus caused by the deformation of the previous element (Ravindranath *et al.*, 2011). In the case of the variable-line-spacing grating monochromator the correction can be made without an additional optical element (Reininger *et al.*, 2008).

An extension of a high-repetition-rate laser pump/X-ray probe setup implemented at the Advanced Photon Source

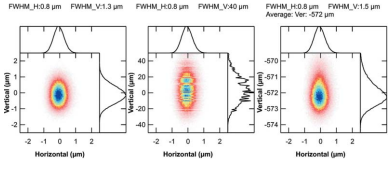

(APS) (March *et al.*, 2011), which requires high X-ray flux but only limited energy resolution such as offered with pink beams, is being developed. The setup is based on a liquid jet operating around 5–6 m s^{-1}, producing a constantly refreshed 100 µm-thick flat target. The X-ray beam is focused to a sub-10 µm spot, probing a laser-excited zone produced by laser spots as small as 25 µm. The X-ray microprobe geometry is essential, since it allows to completely clear a fresh spot in the jet at repetition rates around 300 kHz. The small X-ray beam probes only the center of the laser spot where excitation is maximal and uniform and yields high-excitation fractions with modest laser pulse energies. Conserving the microprobe concept with pink beam is essential, as is the ability to tune the central photon energy and reject higher harmonics from the undulator radiation. Tunability in the 5–10 keV range, where all *K*-edges of first-row transition metals fall, separated by 500–600 eV, is necessary to keep the element specificity of hard X-ray spectroscopies that allow for local probing around an active center. Harmonic rejection is also essential for the element specificity and to eliminate higher-order electronic excitations that would contaminate the signal. The requirements of this experiment can be fulfilled with the simple optical system described below. The experiment and its detectors should be on a single movable platform capable of translating fractions of a millimeter in the focal plane to compensate for the small movement of the focus resulting from the angular change required to compensate the heat-load-induced deformation at a given undulator setting.

2. Source and beamline

The calculations presented in this paper were performed for an undulator beamline at the APS and for one to be installed after the APS has been upgraded to a multibend achromat lattice (Decker, 2014). The optical system is designed to address the following requirements: (i) highest possible flux in the energy range 5–10 keV, (ii) minimal high harmonic contamination, and (iii) a spot size not larger than 10 µm in both directions.

The sources used in the calculations were a 2.4 m-long 3.3 cm-period undulator installed in one of the straight sections of the APS (sector 7) and a 2.6 cm-period undulator of the same length installed at one of the straight sections of the upgraded APS (APSU). The electron energy of the upgraded storage ring will be reduced from 7 GeV to 6 GeV and the stored current increased from 100 mA to 200 mA. The sizes and divergences of the electron beam at the APS and the expected values at the APSU in timing mode (Decker, 2014), as well as the values convoluted with those of the single electron emission from the undulators when tuned to 5 keV, 6.5 keV and 10 keV, are listed in Table 1. The table shows that the horizontal emittance planned for the upgrade will be reduced by a factor of 65.

The lower panel in Fig. 1 shows the spectra of the 2.6 cm-period undulator at the APSU through an angular aperture of 38 µrad × 38 µrad when the first harmonic is tuned to 5 keV, 6.5 keV and 10 keV. The full width at half-maximum (FWHM) of the first harmonics in Fig. 1 are 119 eV at 5 keV, 192 eV at 6.5 keV and 433 eV at 10 keV. The flux values in the figures are normalized to these FWHM values. As seen in these three traces, the flux (for the respective FWHM) is higher than 4 × 10^{16} photons s^{-1}. The corresponding values for the 3.3 cm-period undulator at the APS for the same angular aperture are 165 eV at 5 keV, 262 eV at 6.5 keV and 570 eV at 10 keV. The flux in each case is lower than in the APSU due to the higher current in the ring, the lower emittance and the increase in the number of undulator periods in the APSU. The flux curves described above were obtained using the *SPECTRA* (10.0) code (Tanaka & Kitamura, 2001).

Table 1
Sizes and divergences of the electron beam and convoluted sizes and divergences of the electron beam with the single electron emission at 5, 6.5 and 10 keV.

P: present APS. U: APS upgrade timing mode.

	Electron P/U	5 keV P/U	6.5 keV P/U	10 keV P/U
Horizontal size (µm)	275/18	275/19	275/18	275/18
Vertical size (µm)	10/10	11/12	11/11	10/11
Horizontal divergence (µrad)	11/2.6	13/7.6	13/6.8	12/5.7
Vertical divergence (µrad)	3.5/4.3	8.0/8.4	7.2/7.6	6.2/6.7

The optical system consists of two meridional elliptical cylinders in a Kirkpatrick–Baez (KB) configuration. The first mirror of the KB system deflects and focuses in the vertical direction. The second mirror deflects and focuses in the horizontal direction. The first mirror (M1) is at a grazing angle

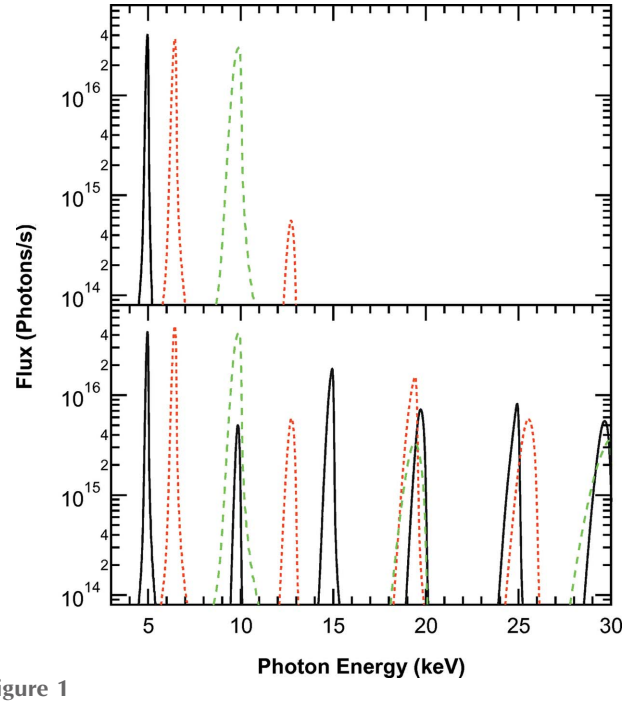

Figure 1
Undulator spectra (APS upgrade, 2.6 cm-period) normalized to the FWHM of the first harmonic in each trace. Upper (lower) panel: after (before) reflections from the M1 and M2 mirrors. Solid (black) line: undulator tuned to 5 keV and mirrors coated with C. Dotted (red) line: undulator tuned to 6.5 keV and mirrors coated with Rh. Dashed (green) line: undulator tuned to 10 keV and mirrors coated with Rh.

of incidence of 5 mrad and has two optical coatings along its length, one with Rh and the other with C. The second mirror (M2) is at a grazing angle of incidence of 6 mrad and has the same coatings. We have chosen different angles of incidence on M1 and M2 to have higher flexibility on the higher-order suppression by using different coatings on the mirrors. Both mirrors are assumed to be side-cooled with water and are 300 mm long. The first and second mirror are located at 35.0 m and 35.5 m from the source, respectively. Their common focus is located 0.5 m downstream from the center of M2 allowing for a relatively large working distance.

The C reflective coatings suppress the higher harmonics in the energy range around 5 keV with very high reflectivity. The energy range between 6.5 and 11.5 keV is covered by the Rh coatings with reasonable second-order suppression, approximately one order of magnitude at 6.5 keV increasing to over two orders of magnitude at 7.5 keV. The lower panel in Fig. 1 shows the spectra before the reflections and the upper panel shows the spectra after the two reflections, revealing the efficient higher-order suppression and the fact that the two reflections decrease the flux by less than 30%. A significantly better higher-order suppression around 6.5 keV could be obtained by using C on M1 and Rh on M2 at the expense of flux.

3. Absorbed power and finite-elements results

The absorbed power and absorbed power density on the optics were obtained using the *SRCalc* code (Reininger, 2001). Those results, represented by the narrow line along the M1 mirror center in Fig. 2, were used to calculate the mirror's deformation using ANSYS® (release 15.0). The mirror was modeled in ANSYS® (see Fig. 2) as a flat Si block, 300 mm long, 50 mm tall and 50 mm wide, sandwiched between two OFHC copper plates, 300 mm long, 45 mm tall and 12.7 mm wide. Each of the two copper plates has a groove for a cooling copper tube with 9.5 mm outer diameter. The thermal conductance between the Si and Cu (with In foil in between) was assumed as 8000 W m^{-2} K^{-1} (Khounsary *et al.*, 1997) (note the labeling in their Fig. 5 is incorrect). The cooling water was assumed to be at 298.6 K, while the cooling coefficient at the copper–water interface was assumed to be 2000 W m^{-2} K^{-1} (Incropera, 2006). Since the temperature change in all cases was only a few degrees, the Young's modulus and Poisson's ratio were assumed to be constant in the analysis, 169 Mpa and 0.182, respectively. The resultant maximum Von Mizes stress is 5.9 MPa, orders of magnitude less than failure stress in Si (Petersen, 1982).

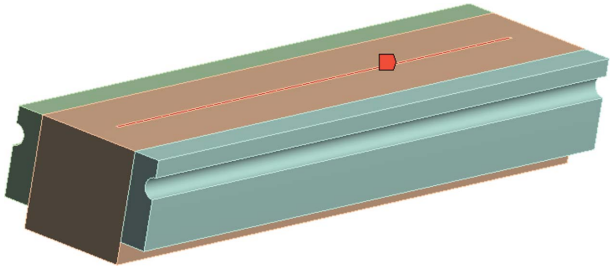

Figure 2
Model of the mirrors used in the finite-element calculations (see text).

Table 2
Power and maximum power density (MPD) absorbed by M1 and M2 when the undulators are tuned to 5, 6.5 and 10 keV.

P: present APS. U: APS upgrade timing mode.

Energy (keV)	Coating	M1 total power (W) P/U	M1 MPD (mW mm^{-2}) P/U	M2 total power (W) P/U	M2 MPD (mW mm^{-2}) P/U
5	C	152/245	410/670	1.1/1.7	13/15
6.5	Rh	97/156	270/450	15/20	180/320
10	Rh	38/44	110/140	6.9/13	60/110

The absorbed power densities were calculated for the two different sources when the undulators were tuned to several energies between 5 and 10 keV. The carbon coating was assumed on both optical elements for energies lower than 6.5 keV and the Rh coating was assumed on the mirrors for energies higher than or equal to 6.5 keV. Evidently, the highest power and power density absorbed by M1 is when the undulators are tuned to 5 keV. The maximum power and power density absorbed by M2 is significantly lower than that absorbed by M1 and occurs when the undulators are tuned to 6.5 keV. Table 2 lists the absorbed power and power densities absorbed by the two mirrors in the APS and APSU cases when the undulators are tuned to 5, 6.5 and 10 keV. The table shows that the total power and absorbed power densities will be higher in the APSU case.

Finite-element analysis of the mirrors' deformations due to the absorbed power with the cooling scheme described above were performed for most of the cases listed in Table 2 relative to their ideal elliptical cylinder surfaces. The largest deformation of the M1 mirror occurs when the stripe with the C coating is exposed to the radiation emitted from the 2.6 cm-period APSU undulator tuned to 5 keV, the case where the mirror absorbs the highest power (see Table 2). Even in this case (see Fig. 3) the mirror is mostly bent along its length with

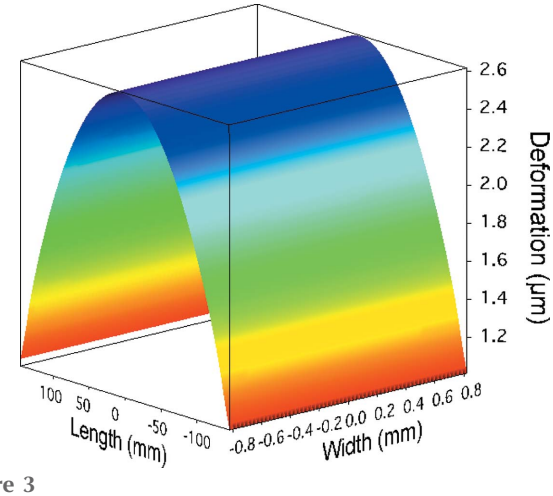

Figure 3
Results of the ANSYS® model for the case where the M1 mirror absorbs the power emitted by the 2.6 cm undulator (APSU) when tuned to 5 keV.

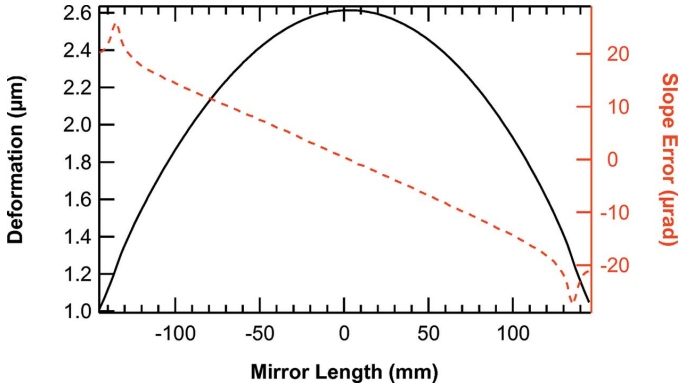

Figure 4
Deformation and slope error along the M1 mirror length at its center obtained from the results shown in Fig. 3.

practically no deformation along the width of the illuminated area where the power is absorbed. Fig. 4 shows the deformation and slope of the mirror along its length at the mirror center obtained from the data shown in Fig. 3. Clearly, the slope is almost linear over the full mirror length except at the edges where the absorbed power is zero. The transition from the illuminated to the non-illuminated portion is seen in the slope change at ± 130 mm. From a linear fit to the slope one finds that the mirror radius of curvature over the linear region is convex and almost constant ($\simeq -6.5$ km). Similar bending to a convex cylinder with larger radius of curvature was obtained for the other cases investigated. With the help of the lens formula one obtains a focal length equal to -6.5 km $\times$ $\sin(0.005)/2 = -16.2$ m, implying that the effect of the absorbed power density is to create a virtual source for the mirror located at 11.1 m (upstream from the mirror) rather than at 35 m. The finite-element results for the deformation of the M1 mirror for the cases listed in Table 2 translate into a virtual source between 11.1 m and 27 m. The corresponding change in the source position of the M2 mirror is significantly smaller than that for the M1 mirror, a shift of only 1.0 m, which occurs when the 2.6 cm-period undulator (APSU) is tuned to 6.5 keV.

4. Ray tracings

A series of ray tracings using the *SHADOW* code (Sanchez del Rio *et al.*, 2011; Lai & Cerrina, 1986) were performed for the photon energies listed in Table 1 using the beam parameters of the 3.3 mm-period (APS) and the 2.6 mm-period (APSU) undulator. The source size and divergences were assumed to be Gaussians using the RMS values listed in Table 1. The optical system included the two meridional elliptical cylinder mirrors mentioned in §2 at the distances indicated in that section. The ray tracings include slope errors with an RMS value of 0.2 μrad (RMS figure error of 4.4 nm) on both mirrors which contribute to a FWHM size at the focus equal to 0.47 μm ($2 \times 2.35 \times 0.2$ μrad $\times$ 500 mm) along the horizontal direction and 0.94 μm along the vertical direction. These slope errors, as well as the additional effect due to the heat-load-induced deformation, were prepared for the ray tracings with the PRESURFACE routine in *SHADOW*.

Fig. 5 shows the ray tracing results obtained when the APSU undulator is tuned to 5 keV. We recall that this is the case where M1 absorbs the highest power and power density (see Table 2) and whose deformation due to the absorbed power is shown in Fig. 3. The left-hand panel in the figure shows the image at the focal plane including the 0.2 μrad RMS slope error. The FWHMs of the spot sizes given in the figure agree with those obtained from the square root of the sum of the squares of the demagnified FWHM source (0.63 μm horizontal and 0.82 μm vertical) and the FWHM size due to the slope errors. The middle panel displays the case that also includes the deformation due to the absorbed power on M1 and M2. The effect of the absorbed power along the vertical direction is significant; it increases the FWHM from 1.3 μm to 40 μm. As expected, there is practically no increase in the size along the horizontal direction since the total power

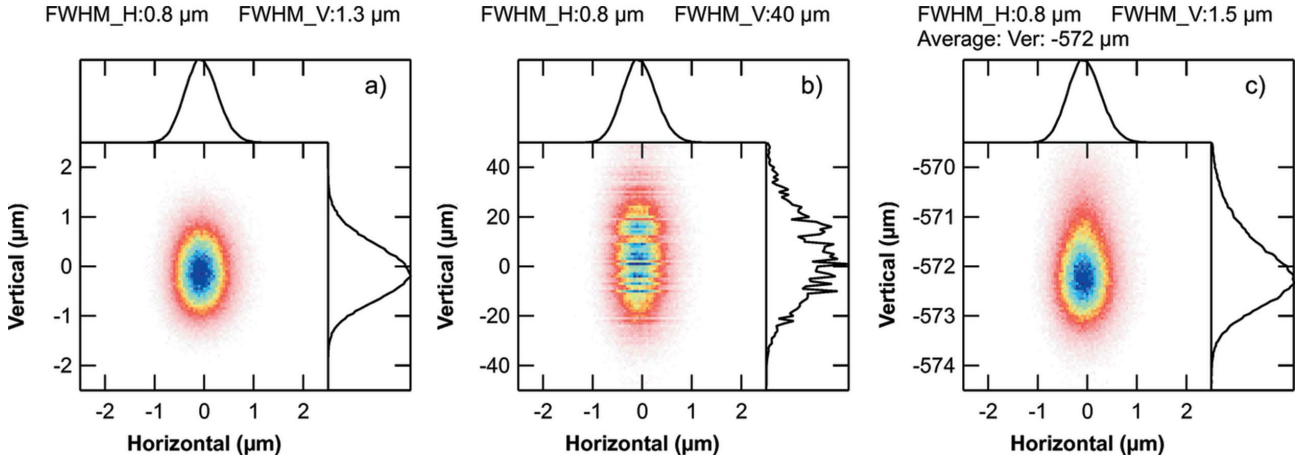

Figure 5
Ray tracings showing the image at the focal plane. The source is a 2.6 cm-period undulator (APSU) tuned to 5 keV. Both M1 and M2 mirrors have a C optical coating. (*a*) Assuming slope errors of 0.2 μrad on both M1 and M2. (*b*) Including the slope errors and the deformation due to the absorbed power. (*c*) As in (*b*) after a pitch correction of 288 μrad. Note that the vertical ranges in (*a*) and (*c*) are the same but the beam is shifted.

and power densities absorbed by M2 are very low in this case (see Table 2). Evidently, the image blurring along the vertical direction is beyond the experimental requirement. As mentioned in the previous section, the effect of the mirror deformation is practically a shift in the source position. A 'correction' to the defocus can be achieved by simply changing the angle of incidence on the M1 mirror. A simple calculation based on the assumption that M1 is a meridional cylindrical mirror (and not a meridional elliptical cylinder) with an entrance arm of 11.1 m and an exit arm of 1 m shows that the defocus term is zeroed when the grazing angle of incidence is decreased from 5 mrad to 4.72 mrad. The right-hand panel in Fig. 5 shows the image at the focal plane after decreasing the pitch of the mirror by 0.288 mrad, which decreases the FWHM along the vertical direction to 1.5 µm. Clearly, the change in pitch corrected the defocus but leaves a slight coma aberration (seen in the image asymmetry along the vertical direction, which is not observed in the left-hand panel). The deviation between the calculated change in angle pitch and the optimized value used in the ray tracings is due to the optimization trying to reduce the spot size enlarged by both the defocus and the coma. Obviously, the change in pitch translates the beam in the focal plane by 0.57 mm vertically, which can be easily corrected in experiments that do not require energy scanning. A cooled bendable mirror could also be used to compensate for the change in the source position induced by the absorbed heat load; its main advantage is the fact that the angle of incidence is kept constant. To the best of our knowledge, a cooled mirror bendable to an elliptical cylinder absorbing the power described in Table 2 and focusing to a 1.5 µm spot has not been reported in the literature.

The case presented above is the worst in terms of absorbed power density for the M1 mirror in the energy range 5–10 keV. The worst case for the M2 mirror is when the APSU undulator is tuned to 6.5 keV and the Rh coating is used on the mirrors. In this case (see Fig. 6), the FWHMs of the image along the horizontal and vertical directions increase from 0.7 µm to 0.84 µm and from 1.3 µm to 36 µm, respectively. From the results of the finite-element analyses one obtains that the vertical virtual source is at 15.6 m and the horizontal virtual source is at 34 m. The simple calculations for the required correction yield an angle change of −168 µrad for M1 and 3.5 µrad for M2. Using slightly different angles on M1 (−179 µrad) and M2 (3.2 µrad) reduces the FWHM to 0.7 µm for the horizontal and 1.4 µm for the vertical. The translation of the beam in the focal plane after the corrections is 6.3 µm horizontal and 358 µm vertical.

The optical configuration presented here was chosen to fulfil the requirements described in §1 when using the 3.3 cm undulator at the APS. Evidently, the demagnified horizontal source is practically not changed by the deformation of the M2 mirror. Its value has a FWHM of 7.4 µm fulfilling the experimental requirements. Along the vertical direction the absorbed heat load and the deformations are similar to the cases for the APSU. When the undulator is tuned to 5 keV a change in the pitch angle of 180 µrad on M1 is required to reduce the FWHM vertical size from 29 µm to 1.6 µm. We also simulated the case when the 3.3 cm-period device at the APS is tuned to 3 keV and were able to reduce the spot size due to the absorbed power from a FWHM of 28 µm down to 1.9 µm.

5. Discussion

We have described a simple optical system capable of correcting the strong defocus caused by the deformation of the mirrors due to the absorbed power emitted by an undulator. The system will deliver at least 70% of the photons emitted by an insertion device in the first harmonic without higher-order contamination when the insertion device is tuned for energies between 5 and 10 keV. The scheme presented here can focus down to micrometer size despite the fact that the first mirror absorbs up to 245 W. Smaller working distances should allow for higher demagnification and therefore to spot sizes below a micrometer. With the appropriate coatings and incidence

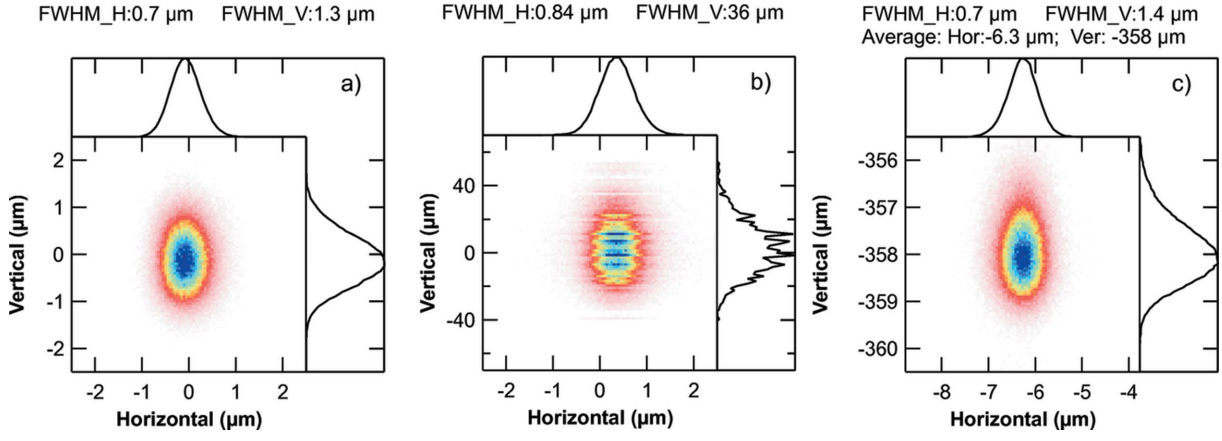

Figure 6
Ray tracings showing the image at the focal plane. The source is a 2.6 cm-period undulator (APSU) tuned to 6.5 keV. Both M1 and M2 mirrors have a Rh optical coating. (*a*) Assuming slope errors of 0.2 µrad on both M1 and M2. (*b*) Including the slope errors and the deformation due to the absorbed power in both mirrors. (*c*) As in (*b*) after a pitch correction of 179 µrad on M1 and 3.2 µrad in M2. Note that the vertical ranges in (*a*) and (*c*) are the same but the beam is shifted.

angles on the mirrors this simple system could cover other energy ranges. The very high flux, spectral purity and small spot achievable with this system makes it most suitable for photon-hungry experiments.

Acknowledgements

The Advanced Photon Source, an Office of Science User Facility operated for the US Department of Energy (DOE) Office of Science by Argonne National Laboratory, was supported by the US DOE under Contract No. DE-AC02-06CH11357. LY acknowledges support from from the US Department of Energy (DOE) Office of Science, Division of Chemical, Geological and Biological Sciences under Contract No. DEAC02-06CH11357.

References

Bohic, S., Simionovici, A., Snigirev, A., Ortega, R., Devès, G., Heymann, D. & Schroer, C. G. (2001). *Appl. Phys. Lett.* **78**, 3544–3546.

Cocco, D., Bortoletto, G., Sergo, R., Sostero, G. & Cudin, I. (2010). *Nucl. Instrum. Methods Phys. Res. A*, **616**, 128–133.

Coppens, P., Benedict, J., Messerschmidt, M., Novozhilova, I., Graber, T., Chen, Y.-S., Vorontsov, I., Scheins, S. & Zheng, S.-L. (2010). *Acta Cryst.* A**66**, 179–188.

Decker, G. (2014). *Synchrotron Radiat. News*, **27**, 13–17.

Elleaume, P. (1992). *Rev. Sci. Instrum.* **63**, 321.

Eybert, L., Wulff, M., Reichenbach, W., Plech, A., Schotte, F., Gagliardini, E., Zhang, L., Hignette, O., Rommeveaux, A. & Freund, A. K. (2002). *International Symposiumon Optical Science and Technology*, edited by A. K. Freund, A. T. Macrander, T. Ishikawa and J. L. Wood, pp. 246–257. SPIE.

Graber, T., Anderson, S., Brewer, H., Chen, Y.-S., Cho, H. S., Dashdorj, N., Henning, R. W., Kosheleva, I., Macha, G., Meron, M., Pahl, R., Ren, Z., Ruan, S., Schotte, F., Srajer, V., Viccaro, P. J., Westferro, F., Anfinrud, P. & Moffat, K. (2011). *J. Synchrotron Rad.* **18**, 658–670.

Idir, M., Mercere, P., Modi, M. H., Dovillaire, G., Levecq, X., Bucourt, S., Escolano, L. & Sauvageot, P. (2010). *Nucl. Instrum. Methods Phys. Res. A*, **616**, 162–171.

Incropera, F. P. (2006). *Fundamentals of Heat and Mass Transfer*, 6th ed. New York: Wiley,

Khounsary, A. M., Chojnowski, D., Assoufid, L. & Worek, W. M. (1997). *Thermal Contact Resistance Across a Copper–Silicon Interface*, edited by A. T. Macrander and A. M. Khounsary, pp. 45–51. SPIE.

Kohn, V. G., Argunova, T. S. & Je, J. H. (2013). *AIP Adv.* **3**, 122109.

Kosior, E., Bohic, S., Suhonen, H., Ortega, R., Devès, G., Carmona, A., Marchi, F., Guillet, J. F. & Cloetens, P. (2012). *J. Struct. Biol.* **177**, 239–247.

Lai, B. & Cerrina, F. (1986). *Nucl. Instrum. Methods Phys. Res. A*, **246**, 337–341.

March, A. M., Assefa, T. A., Bressler, C., Doumy, G., Galler, A., Gawelda, W., Kanter, E. P., Nemeth, Z., Papai, M., Southworth, S. H., Young, L. & Vanko, G. (2015). *J. Phys. Chem.* Submitted.

March, A. M., Stickrath, A., Doumy, G., Kanter, E. P., Krässig, B., Southworth, S. H., Attenkofer, K., Kurtz, C. A., Chen, L. X. & Young, L. (2011). *Rev. Sci. Instrum.* **82**, 073110.

Petersen, K. E. (1982). *Proc. IEEE*, **70**, 420–457.

Rau, C., Crecea, V., Liu, W., Richter, C. P., Peterson, K. M., Jemian, P. R., Neuhäusler, U., Schneider, G., Yu, X., Braun, P. V., Chiang, T. C. & Robinson, I. K. (2007). *Nucl. Instrum. Methods Phys. Res. B*, **261**, 850–854.

Ravindranath, V., Sharma, S., Reininger, R. & Wang, N. (2011). *Diamond Light Source Proc.* **1**, e55.

Reininger, R. (2001). *SRCalc.* Unpublished.

Reininger, R., Kriesel, K., Hulbert, S. L., Sanchez-Hanke, C. & Arena, D. A. (2008). *Rev. Sci. Instrum.* **79**, 033108.

Sanchez del Rio, M., Canestrari, N., Jiang, F. & Cerrina, F. (2011). *J. Synchrotron Rad.* **18**, 708–716.

Shen, G., Chow, P., Xiao, Y., Sinogeikin, S., Meng, Y., Yang, W., Liermann, H.-P., Shebanova, O., Rod, E., Bommannavar, A. & Mao, H.-K. (2008). *High Press. Res.* **28**, 145–162.

Susini, J., Marot, G. G., Zhang, L., Ravelet, R. & Jagourel, P. (1992). *Rev. Sci. Instrum.* **63**, 489–492.

Sutter, J., Alcock, S. & Sawhney, K. (2012). *J. Synchrotron Rad.* **19**, 960–968.

Tanaka, T. & Kitamura, H. (2001). *J. Synchrotron Rad.* **8**, 1221–1228.